



Contact line length dominance in evaporation of confined nonspherical droplets

Gun Oh ^{1,2}, Jae-Hong Lim,³ Sung Hoon Kang ^{2,*} and Byung Mook Weon ^{1,4,†}

¹*Soft Matter Physics Laboratory, School of Advanced Materials Science and Engineering, SKKU Advanced Institute of Nanotechnology (SAINT), Sungkyunkwan University, Suwon 16419, Republic of Korea*

²*Department of Mechanical Engineering and Hopkins Extreme Materials Institute, Johns Hopkins University, Baltimore, Maryland 21218, USA*

³*Pohang Accelerator Laboratory, POSTECH, 80 Jigokro-127-beongil, Nam-gu, Pohang, Gyeongbuk 37673, Republic of Korea*

⁴*Research Center for Advanced Materials Technology, Sungkyunkwan University, Suwon 16419, Republic of Korea*



(Received 18 September 2023; accepted 10 January 2024; published 8 February 2024)

Free droplets are spherical within capillary lengths and become nonspherical when trapped in a confined space. Confined nonspherical droplets are as common as spherical droplets. Yet, their evaporation dynamics are not fully understood because of their geometrical complexity. We use monochromatic synchrotron x-ray microtomography to investigate the evaporation dynamics of confined nonspherical water droplets trapped by micropillars based on three-dimensional geometrical information with time. We find two types of confined nonspherical droplets: Wenzel droplets with single-sided air-water interfaces, and Cassie-Baxter droplets with double-sided interfaces. Both droplets show similar sphericity at large volumes but approach different ones at small volumes: Wenzel droplets follow a thin film limit, whereas Cassie-Baxter droplets follow a spherical sessile limit. Despite the geometrical complexity of confined nonspherical droplets, the vapor diffusion mechanism suggests that the evaporative flux is maximal at the contact line, which governs the evaporation dynamics, as proven by observations. The proportionality of the evaporation rate to the contact line length demonstrates the contact-line-length-dominant evaporation dynamics of confined nonspherical droplets. The findings of this study can unify the evaporation mechanism for spherical sessile and confined nonspherical droplets, even with geometric complexity.

DOI: [10.1103/PhysRevResearch.6.L012026](https://doi.org/10.1103/PhysRevResearch.6.L012026)

Introduction. Droplet evaporation is a fundamental process in nature [1–9], inkjet printing [10–12], painting [13], and biofabrication [14–18]. The dynamics of droplet evaporation are well understood if droplets are spherical or capillarity predominates [19,20]. The vapor diffusion mechanism successfully describes and predicts the evaporation rates of spherical sessile droplets, with the evaporative flux J proportional to the vapor diffusivity D times the vapor concentration gradient dc/dn [21–24]. Spherical droplets are standard when the droplet is smaller than the capillary length $\lambda_c = (\gamma/\Delta\rho g)^{1/2}$, where γ is the surface tension of the fluid interface, $\Delta\rho$ is the mass density difference of the fluids, and g is the gravitational acceleration; $\lambda_c = 2.7$ mm for water at room temperature, $T = 25$ °C. However, nonspherical droplets are more general than spherical droplets when trapped in a confined space [25–27]. Although they are common, the evaporation dynamics of confined nonspherical

droplets are little understood due to their geometrical complexity [27–29].

Visualizing and quantifying the geometrical complexity of confined nonspherical droplets are crucial to identifying their evaporation dynamics. Thus, we adopt microtomography with monochromatic synchrotron x-ray to investigate the complex geometry and evaporation dynamics of confined nonspherical water droplets within capillary lengths trapped by micropillars. Due to the high penetration capability of x-rays, we can acquire two-dimensional (2D) projection images to analyze fluid evaporation on a substrate [30] or fluid geometry trapped inside porous media (such as soil or fabric) [31,32]. Moreover, we can successfully obtain three-dimensional (3D) geometrical information of complicated droplets based on 2D projection images from samples with several millimeter thicknesses [33]. Acquiring 3D geometrical details is essential to understanding the time-sequential behavior of confined nonspherical droplets during evaporation [27], which is difficult with conventional imaging techniques. The fast image acquisition capability (spending four seconds for a 3D image) of synchrotron x-ray microtomography makes it suitable for our study, particularly for observing the rapid evaporation dynamics of microliter-scale water droplets within capillary lengths (spending 1000 seconds for complete evaporation) [34–36].

This study demonstrates how the vapor diffusion dynamics govern the evaporation dynamics of confined nonspherical

*shkang@jhu.edu

†bmweon@skku.edu

Published by the American Physical Society under the terms of the [Creative Commons Attribution 4.0 International](https://creativecommons.org/licenses/by/4.0/) license. Further distribution of this work must maintain attribution to the author(s) and the published article's title, journal citation, and DOI.

droplets. Using x-ray microtomography, we quantify the time dependences of the contact line length (L), the surface area (S), and the volume (V) of confined nonspherical droplets within capillary lengths when trapped by micropillars. Furthermore, considering the entire droplet surface (air-water and water-resin) (S_e) and the total droplet volume (V), we calculated the droplet sphericity as $\Psi = \pi^{1/3}(6V)^{2/3}/S_e$. These direct observations show two distinct types of confined nonspherical droplets: Wenzel [37] droplets with single-sided air-water interfaces and Cassie-Baxter [38] droplets with double-sided interfaces. We demonstrate that the evaporation rates of confined water droplets are proportional to the total lengths of the contact lines. Both droplets show similar sphericity at large volumes but approach different ones at small volumes: Wenzel droplets follow a thin film limit, whereas Cassie-Baxter droplets follow a spherical sessile limit. This finding offers clear evidence of the possibility of universality in droplet evaporation dynamics, even for confined nonspherical droplets with complex geometry.

The evaporation dynamics of confined nonspherical droplets must depend on the surface area or the contact line length because of the escape of water vapor molecules from liquid water surfaces [9,39]. The central question is to identify which contributes more to the evaporation of confined nonspherical droplets between the surface area and the contact line length. The contact line length dominance results from the nonuniform evaporation flux mainly escaping from the contact line, while the surface area dominance results from the uniform evaporation flux on the droplet surface.

Experiments. We fabricated micropillar-patterned substrates to form confined nonspherical droplets within capillary lengths, in which small-volume ($1.0 \sim 1.5 \mu\text{L}$) water could be trapped among vertical micropillars (Fig. S1 within the Supplemental Material [40]). The micropillar-patterned substrates were made of resin (Surgical Guide, Formlabs, USA) by a 3D printer (Form 2, Formlabs, USA; with a resolution of $50 \mu\text{m}$). The micropillars had a diameter (d) of $350 \mu\text{m}$, a pitch (p) of $300 \mu\text{m}$, and a height (h) of $1500 \mu\text{m}$. The substrate surface was hydrophilic (45° for the water contact angle). We used deionized water (Classic DI MK2, ELGA, UK) as the model solvent for the droplets.

Visualizing and quantifying the geometrical complexity of confined nonspherical droplets are essential in identifying their geometrical information. High-resolution spatial and temporal information on the droplet contact line length, the droplet surface area, and the droplet volume is crucial to evaluate their evaporation dynamics. X-ray microtomography with fast image acquisition is needed for this purpose. We used the 6C Biomedical Imaging (BMI) beamline in the Pohang Light Source II (PLS-II), providing monochromatic synchrotron x-ray with 35 keV photon energy [27,30,34]. The beamline included a scintillator (LuAG: Ce $50 \mu\text{m}$), a ten-magnification lens coupled with an sCMOS (scientific complementary metal-oxide-semiconductor; PCO Edge 5.5, PCO Imaging, Germany) camera with a pixel size of $0.65 \mu\text{m}$ and a field of view of $1.6 \text{ mm} \times 1.4 \text{ mm}$. The exposure time for each 2D projection image was 20 ms , and the total number of projection images for each microtomography set was 200 taken from on-the-fly scanning within 180° , eventually requiring four seconds for one microtomography set

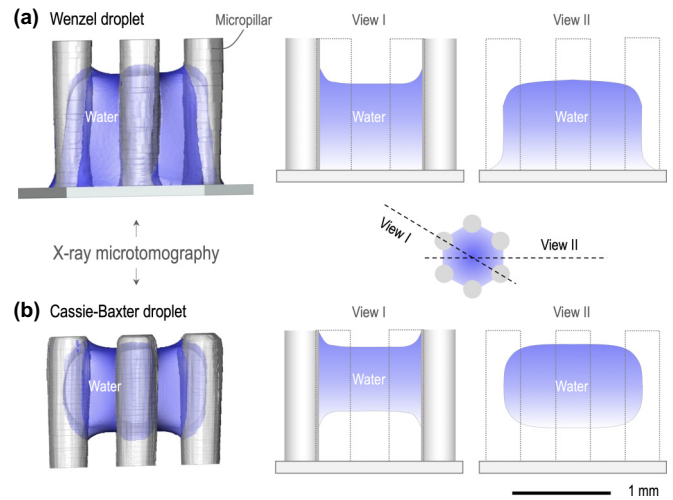


FIG. 1. Confined nonspherical droplets with geometric complexity. (a) Wenzel droplets: a $1.5 \mu\text{L}$ droplet sunk to the substrate bottom. (b) Cassie-Baxter droplets: a $1.0 \mu\text{L}$ droplet floated among hexagonally arrayed micropillars. The left images were taken by x-ray microtomography (along view I), the middle schematic images were from view I, and the right were from view II. The formation of Wenzel or Cassie-Baxter droplets depends on the initial droplet volumes because the initial accommodable space surrounded by micropillars was $\sim 1.5 \mu\text{L}$ (see Figs. S1 and S2 within the Supplemental Material [40]).

($20 \text{ ms/projection} \times 200 \text{ projections} = 4 \text{ s}$) that enabled fast image acquisition [27]. The sample stage has a rotation speed of $45^\circ/\text{s}$, which requires 4 s for 180° of rotation. We selected the microtomographic observation interval to be 20 seconds between microtomographic sets.

A total of 30 sets of time-sequential x-ray microtomograms were acquired during the evaporation of confined nonspherical droplets. The 2D projection images obtained were reconstructed with the OCTOPUS software (version 8.9.3, XRE, Ghent, Belgium) to stack the 200 projections to make a complete 3D microtomogram. The reconstructed images were loaded into AVIZO software (version 2020.02, Thermo Fisher Scientific, USA) to segment the microtomogram and measure the triple phase (air-water-resin) contact line length, the air-water surface area, and the droplet volume that defines the geometry of the confined nonspherical droplets. Segmentation of the confined nonspherical water droplets, the resin micropillar-patterned substrates, and the air was possible based on their attenuation coefficient difference depending on the material density and the atomic number. The three components (air, water, and resin) were distinguishable. We measured the total contact line length by counting all pixels along the three-phase contact lines. The entire surface area was measured by calculating the intersection between the water droplet and the air. The droplet volumes were measured by counting all the voxels in the droplets. In addition, we counted the entire droplet surface (air-water and water-resin) for the calculation of droplet sphericity as $\Psi = \pi^{1/3}(6V)^{2/3}/S_e$.

Results. Two distinct types of confined nonspherical water droplets were observed, as illustrated in Fig. 1. The initially small volume ($1.0 \sim 1.5 \mu\text{L}$) of water can be trapped among

the micropillars because the initial accommodable space surrounded by micropillars is $1.5 \mu\text{L}$ (Figs. S1 and S2 within the Supplemental Material [40]). The substrate surface is hydrophilic (45° for the water contact angle). The first type of confined nonspherical water droplet is the Wenzel droplet which has a single-sided air-water interface and touches the substrate (Fig. 1(a), and Movies S1 and S3 within the Supplemental Material [40]). The second type is the Cassie-Baxter droplet which has double-sided air-water interfaces and floats above the substrate (Fig. 1(b), and Movies S2 and S4 within the Supplemental Material [40]). The formation of Wenzel or Cassie-Baxter water droplets depends on their initial volumes (V_i): Wenzel droplets are generated at $V_i > 1.5 \mu\text{L}$, whereas Cassie-Baxter droplets at $V_i < 1.5 \mu\text{L}$ because the initial empty volume surrounded by six neighboring micropillars is $1.5 \mu\text{L}$ (Fig. S1 within the Supplemental Material [40]). The geometrical complexity of confined nonspherical water droplets is visualized by x-ray microtomography, providing exact measurements of the contact line length between water and micropillars, the surface area of air-water and micropillars-water interfaces, and the volume of confined nonspherical water shapes.

The fast image acquisition of x-ray microtomography enables time-resolved observations to identify the time evolution of evaporating confined nonspherical water droplets with considerable geometrical complexity. The evaporation dynamics of confined Wenzel and Cassie-Baxter droplets are described in Fig. 2, showing a clear difference at the end of evaporation. The height of a Wenzel droplet continuously and gradually decreases with time ($t/t_f = 0.2 \sim 0.92$, Movie S5 within the Supplemental Material [40]). In contrast, the height of a Cassie-Baxter droplet initially decreases with time ($t/t_f = 0.2 \sim 0.3$), but the droplet later detaches from some of the contacting micropillars ($t/t_f = 0.4 \sim 0.99$, Movie S6 within the Supplemental Material [40]). This phenomenon of confined nonspherical droplets separating from micropillars is found only with the Cassie-Baxter droplet. The droplet detachment would be related to the rupture dynamics of the thin water volume [41,42].

We suggest simple cross-sectional schematic illustration in Fig. 3 based on our observations. The critical initial volume for the Cassie-Baxter and the Wenzel droplets is $V_i^* \sim 1.5 \mu\text{L}$. At the early stages, the Wenzel droplet ($V_i > 1.5 \mu\text{L}$) has a vertically asymmetric cross section, and the Cassie-Baxter droplet ($V_i < 1.5 \mu\text{L}$) has a vertically symmetric cross section (Fig. S2 within the Supplemental Material [40]). Both have a similar geometric relation between the height (h) and the width (w), where the height gradually decreases with time while the width is invariant during evaporation (Fig. S3 within the Supplemental Material [40]). In the late stages, they approach different geometrical limits. The Wenzel droplet reaches a thin film limit, where the height is ultimately small while the width is almost invariant. The Cassie-Baxter droplet has a spherical sessile limit, where the height and the width decrease simultaneously by retraction, and thus, eventually a single spherical sessile droplet remains on a little curved surface. The confined nonspherical water droplets have different geometrical limits depending on the initial droplet volume with respect to the available space.

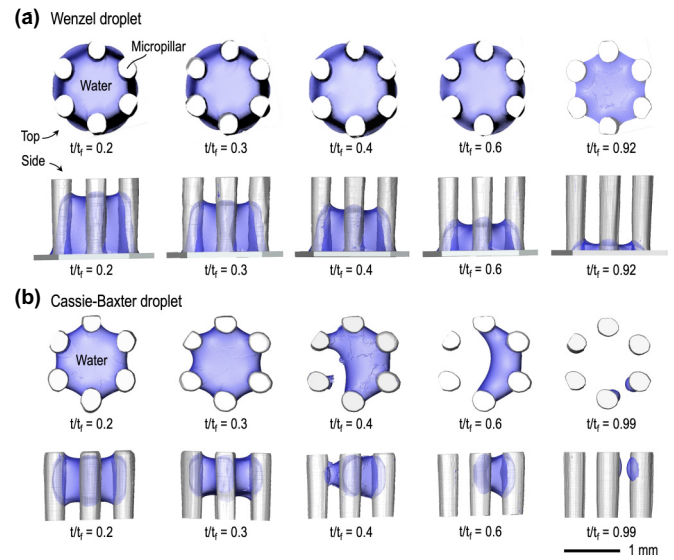


FIG. 2. Evaporation dynamics of confined nonspherical droplets by time-resolved x-ray microtomography. (a) The time evolution of a Wenzel droplet, taken by x-ray microtomography, shows a gradual height decrease for $t/t_f = 0.2 \sim 0.92$ with no detachments from the micropillars. (b) The time evolution of a Cassie-Baxter droplet, taken by x-ray microtomography, shows a gradual decrease of the height for $t/t_f = 0.2 \sim 0.3$ and detachments from some of the micropillars for $t/t_f = 0.4 \sim 0.99$. The final small volume of a Wenzel droplet near t_f is similar to a thin film with a specific upper surface area and a minimal thickness (a thin film limit). In contrast, a last tiny Cassie-Baxter droplet near t_f is similar to a small sessile droplet on a curved surface (a spherical sessile limit).

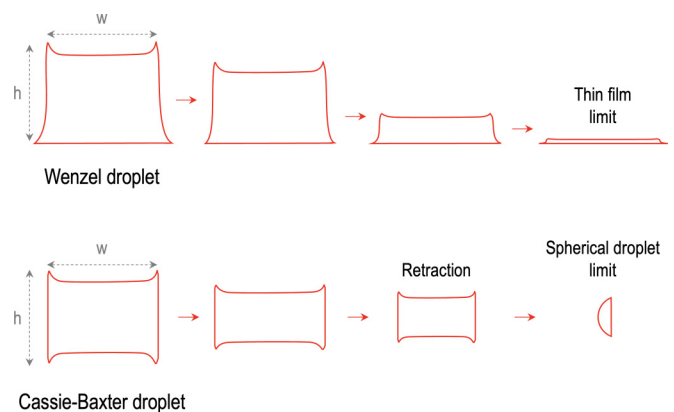


FIG. 3. Cross-sectional schematic illustration. At the early stages, Wenzel droplets (upper) and Cassie-Baxter droplets (lower) have similar geometrical changes between the height (h) and the width (w), where h gradually decreases with time while w is invariant due to the contact line pinning during evaporation. In the late stages, they separately approach different geometrical limits. Wenzel droplets reach a thin film limit, where h is ultimately small while w is almost invariant. Cassie-Baxter droplets reach a spherical sessile limit, where h and w decrease simultaneously by retraction (by detaching from some of the micropillars), and thus eventually, spherical sessile droplets remain on a curved surface of micropillars.

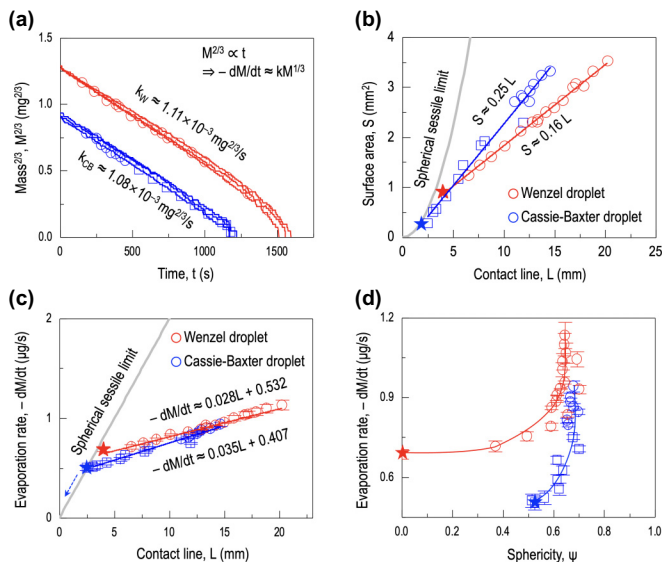


FIG. 4. Contact-line-length-dominant evaporation dynamics. (a) The droplet mass decreases with time, showing the linear $M^{2/3} \propto t$ relations, from $-dM/dt = kM^{1/3}$ in the vapor diffusion mechanism of sessile droplets, where the k values are similar for Wenzel and Cassie-Baxter droplets (marked by the open circle and square for volume data taken with x-ray microtomography and the lines for mass data). All experiments were conducted at $T = 25^\circ\text{C}$ and $RH = 0.3$. (b) The linear $S \propto L$ relations highlight the critical geometry of confined nonspherical droplets (whereas $S \propto L^2$ for spherical sessile droplets, marked by the gray line). The thin film limit is the fate of Wenzel droplets (marked by the red star), and the spherical sessile limit is the fate of Cassie-Baxter droplets (marked by the blue star). (c) The linear $-dM/dt \propto L$ relations look identical between Wenzel and Cassie-Baxter droplets and significantly deviate from spherical sessile droplets (marked by the gray line). (d) The evaporation rates ($-dM/dt$) depend on the sphericity (Ψ) for confined nonspherical droplets, showing that Wenzel and Cassie-Baxter droplets separately approach different geometrical limits in the late stages.

Finally, we demonstrate in Fig. 4(a) (and Fig. S4 within the Supplemental Material [40]) that the droplet mass (or the volume) decreases with time, indicating the approximately linear relations of $\text{mass}^{2/3}$ versus time, which would be similar to the $-dM/dt \approx kM^{1/3}$ relation in the vapor diffusion mechanism of spherical sessile droplets. Here the k values are estimated as $1.11 \times 10^{-3} \text{ mg}^{2/3}/\text{s}$ for Wenzel droplets and $1.08 \times 10^{-3} \text{ mg}^{2/3}/\text{s}$ for Cassie-Baxter droplets (at room temperature, $T = 25^\circ\text{C}$, and relative humidity, $RH = 0.3$). Interestingly, despite the geometrical complexity of confined nonspherical droplets, their evaporation dynamics can be approximated as linear relations between $\text{mass}^{2/3}$ and time. We may find unified evaporation dynamics of confined nonspherical droplets similar to spherical sessile droplets.

Discussion. To get a deep understanding of the evaporation mechanisms of confined nonspherical droplets, we consider the critical geometry of confined nonspherical droplets in Fig. 4(b) by evaluating the linear relations between the contact line length (L) and the surface area (S). We find that

the surface area is linearly proportional to the contact line length ($S \propto L$) for confined nonspherical droplets (marked by the blue and red lines), whereas the surface area is proportional to the square of the contact line length ($S \propto L^2$) for spherical sessile droplets (marked by the gray line). We find $S \approx 0.25L$ (adj. $R^2 = 0.97678$) for Cassie-Baxter droplets and $S \approx 0.16L$ (adj. $R^2 = 0.99607$) for Wenzel droplets (as predicted from $S \propto M^{2/3}$ and $L \propto M^{2/3}$ in Fig. S5 within the Supplemental Material [40]). The linearity of $S \propto L$ is due to the geometrical feature of confined nonspherical droplets in our experiments (while $S \propto L^2$ for spherical sessile droplets). As previously described in Fig. 3, the widths of Wenzel and Cassie-Baxter droplets change little in the early stages of evaporation and can be considered a constant (Fig. S3 within the Supplemental Material [40]). The invariance of the width reduces one dimension, eventually becoming $S \propto L$. The thin film limit is the fate of Wenzel droplets (marked by the red star), as the height is ultimately reducing while the width is kept. The spherical sessile limit is the fate of Cassie-Baxter droplets (marked by the blue star), as the height and the width decrease simultaneously by retraction (by detaching from some of the micropillars), and thus, eventually a single spherical sessile droplet remains on a little curved surface. We show the linear relations between the length of the contact lines and the evaporation rates ($-dM/dt \propto L$), which look identical between Wenzel and Cassie-Baxter droplets [Fig. 4(c)], but significantly deviate from spherical sessile droplets (marked by the gray line), indicating that the contact-line-enhanced vapor diffusion mechanism governs the evaporation dynamics of confined nonspherical droplets (see comparisons in Fig. S6 within the Supplemental Material [40]). The nonzero y intercept in $-dM/dt \propto L$ is attributed to reaching the geometric limit at the final evaporation of confined nonspherical droplets. Consequently, despite the geometrical details of droplets, the vapor-diffusion evaporative flux is maximized at the contact line, which is critical to the evaporation dynamics of droplets, as well known in spherical sessile droplets [4,19,21,43,44]. Significantly, the linear proportionality of the evaporation rate and the contact line length for confined nonspherical droplets are almost identical in Wenzel or Cassie-Baxter droplets, implying that the contact line length would govern the evaporation dynamics. The evaporation dynamics of the Wenzel droplet finishes at the thin film limit, whereas that of the Cassie-Baxter droplet meets the spherical sessile limit and then follows the spherical sessile droplet dynamics.

What causes the main difference between spherical sessile droplets and confined nonspherical droplets? A unified evaporation dynamics originates from the contact line length of droplets: at the same contact line length, the same evaporation rate is expected for confined nonspherical droplets. The actual linearity (slope and intercept) of $-dM/dt \propto L$ is different between spherical sessile and confined nonspherical droplets due to the geometrical difference. The sphericity (Ψ) of confined nonspherical droplets considerably deviates from spherical sessile droplets ($\Psi = 0.55$ at $\theta = 45^\circ$). As shown in Fig. 4(d), the evaporation rates vary with the droplet sphericity, by which Wenzel and Cassie-Baxter droplets approach different geometrical limits in the late stages. Interestingly, at the early evaporation stages of the large-volume droplets,

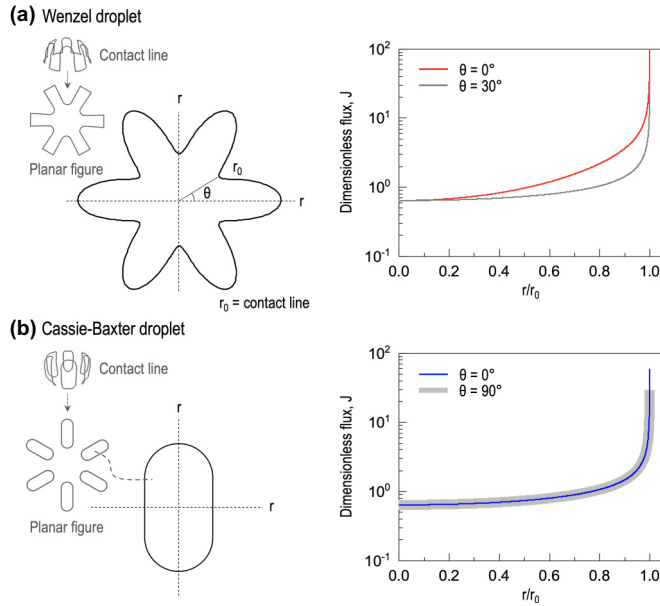


FIG. 5. Contact line geometry. (a) The contact line trajectory of the Wenzel droplet, taken from Fig. 2(a) at $t/t_f = 0.4$, has a hexagonal shape on a curved surface. (b) The contact line trajectory of the Cassie-Baxter droplet, taken from Fig. 2(b) at $t/t_f = 0.2$ [same volumes as (a)], has a summation of six elongated ellipses on a curved surface. Interestingly, the flux is almost the same regardless of the angle in the Cassie-Baxter droplet. The arbitrary position r and θ on a polar coordinate are defined along the air-water interface, and r is normalized by the triple-phase contact line position r_0 . In both cases, the dimensionless evaporative flux J calculated by r and θ in Eq. (1) shows that the evaporative flux diverges at the contact line, regardless of θ .

they show similar sphericity as $\Psi \approx 0.65$, explaining why both confined nonspherical droplets have similar evaporation constants in Fig. 4(a). At the late evaporation stages of the small-volume droplets, Wenzel droplets approach the thin film limit, $\Psi_{th} = 0$, as the volume decreases to zero at the fixed surface area. In contrast, Cassie-Baxter droplets reach the spherical sessile limit, $\Psi_{ss} = 0.55$ (at $\theta = 45^\circ$). This result indicates that the sphericity of droplets can be a critical measure to understand their evaporation dynamics, implying that $kM^{1/3}$ [Fig. 4(a)] should be a function of Ψ [Fig. 4(d)] for confined nonspherical droplets. All evidence suggests the contact-line-length-dominant evaporation mechanism of confined nonspherical droplets. We adopt a previous simulation result that the contact line length governs the vapor diffusion dynamics for polygonal droplets on the flat substrate [24]. The dimensionless evaporative flux $J(r, \theta)$ for confined nonspherical droplets can be described as a function of the position defined r and θ in a polar coordinate:

$$J(r, \theta) = \frac{2}{\pi} \frac{a}{\sqrt{a^2 - r^2}} \{1 + \epsilon f_1(r; n) \cos n\theta + \epsilon^2 [f_{20}(r; n) + f_{22}(r; n) \cos 2n\theta]\}. \quad (1)$$

Here a is a shape parameter defined by the contact line amplitude parameter ϵ and the contact line period number n as $a = a_0(1 + \epsilon \cos n\theta)$ where a_0 is the mean radius [24]. The contact line amplitude parameter varies with the quantity of $\epsilon \sim 0.1$ for hexagonal droplets ($n = 6$) on the flat substrate [24] and $\epsilon \sim 0.4$ on the curved substrate (see details of the ϵ estimation in Fig. S7 within the Supplemental Material [40]). Additionally, $f_1(r; n)$, $f_{20}(r; n)$, and $f_{22}(r; n)$ are solution functions derived from the Green functions [24]. In Fig. 5, we extracted the contact line geometry from x-ray microtomography. The Wenzel droplet from Fig. 2(a) at $t/t_f = 0.4$ shows a continuous hexagonal air-water interface shape. The Cassie-Baxter droplets from Fig. 2(b) at $t/t_f = 0.2$ (at the same volume as the Wenzel droplet) shows a summation of six elongated ellipses. The dimensionless evaporative flux $J(r, \theta)$ calculated by Eq. (1) along the air-water interface indicates that regardless of the detailed geometry, $J(r, \theta)$ diverges at the contact line, suggesting that the contact line length governs the evaporation dynamics. Our experiments demonstrate the dominance of contact line length in the evaporation dynamics of the confined nonspherical droplets at the microliter scales. Our findings need generalization for more complicated geometry with different liquid shapes, such as the fractal-like shape and the grid structure, to be explored in further studies.

Conclusion. We report the evaporation dynamics of confined nonspherical water droplets inside micropillars with geometrical complexity utilizing four-dimensional geometrical information with x-ray microtomography. We find two types of confined nonspherical water droplets by their initial droplet volumes: Wenzel droplets with single-sided air-water interfaces and Cassie-Baxter droplets with double-sided interfaces. Both droplets show similar sphericities at large volumes, but approach to different ones at small volumes: Wenzel droplets follow a thin film limit, whereas Cassie-Baxter droplets follow a spherical sessile limit. Despite the geometrical complexity of confined nonspherical droplets, the vapor diffusion mechanism governs the evaporation dynamics because the evaporative flux diverges at the contact line. Consequently, all evidence supports the proportionality of the evaporation rate to the contact line length for confined nonspherical droplets. This finding proves the contact-line-length-dominant evaporation dynamics of confined nonspherical droplets, with the implication of unifying the evaporation dynamics of spherical sessile droplets and confined nonspherical droplets.

Acknowledgments. This research is supported by the Global Energy Materials Innovator funded by the Korea Institute of Energy Technology Evaluation and Planning (KETEP, 20194010000290), National Research Foundation of Korea (NRF) funded by the Ministry of Education (2019R1A6A1A03033215) and the Ministry of Science and ICT (RS-2022-00143178). S.H.K. would like to thank the support from the Johns Hopkins University Whiting School of Engineering Start-Up Fund and Hanwha Non-Tenured Faculty Award. Experiments at PLS-II were supported in part by MSIT and POSTECH.

- [1] D. Zang, S. Tarafdar, Y. Y. Tarasevich, M. D. Choudhury, and T. Dutta, Evaporation of a droplet: From physics to applications, *Phys. Rep.* **804**, 1 (2019).
- [2] D. Brutin and V. Starov, Recent advances in droplet wetting and evaporation, *Chem. Soc. Rev.* **47**, 558 (2018).
- [3] R. Picknett and R. Bexon, The evaporation of sessile or pendant drops in still air, *J. Colloid Interface Sci.* **61**, 336 (1977).
- [4] R. D. Deegan, O. Bakajin, T. F. Dupont, G. Huber, S. R. Nagel, and T. A. Witten, Capillary flow as the cause of ring stains from dried liquid drops, *Nature (London)* **389**, 827 (1997).
- [5] B. M. Weon and J. H. Je, Capillary force repels coffee-ring effect, *Phys. Rev. E* **82**, 015305(R) (2010).
- [6] J. C. Maxwell, *The Scientific Papers of James Clerk Maxwell* (Cambridge University Press, Cambridge, England, 1890), Vol. 2.
- [7] J. Y. Kim, I. G. Hwang, and B. M. Weon, Evaporation of inclined water droplets, *Sci. Rep.* **7**, 42848 (2017).
- [8] H. Kim, Multiple marangoni flows in a binary mixture sessile droplet, *Phys. Fluids* **34**, 122102 (2022).
- [9] J. K. Im, L. Jeong, J. Crha, P. Trtik, and J. Jeong, High-resolution neutron imaging reveals kinetics of water vapor uptake into a sessile water droplet, *Matter* **4**, 2083 (2021).
- [10] D. Lohse, Fundamental fluid dynamics challenges in inkjet printing, *Annu. Rev. Fluid Mech.* **54**, 349 (2022).
- [11] E. L. Talbot, L. Yang, A. Berson, and C. D. Bain, Control of the particle distribution in inkjet printing through an evaporation-driven sol-gel transition, *ACS Appl. Mater. Interfaces* **6**, 9572 (2014).
- [12] M. Rump, U. Sen, R. Jeurissen, H. Reinten, M. Versluis, D. Lohse, C. Diddens, and T. Segers, Selective evaporation at the nozzle exit in piezoelectric inkjet printing, *Phys. Rev. Appl.* **19**, 054056 (2023).
- [13] R. Zenit, Some fluid mechanical aspects of artistic painting, *Phys. Rev. Fluids* **4**, 110507 (2019).
- [14] I. I. Smalyukh, O. V. Zribi, J. C. Butler, O. D. Lavrentovich, and G. C. L. Wong, Structure and dynamics of liquid crystalline pattern formation in drying droplets of dna, *Phys. Rev. Lett.* **96**, 177801 (2006).
- [15] W.-J. Chung, J.-W. Oh, K. Kwak, B. Y. Lee, J. Meyer, E. Wang, A. Hexemer, and S.-W. Lee, Biomimetic self-templating supramolecular structures, *Nature (London)* **478**, 364 (2011).
- [16] A. Askounis, Y. Takata, K. Sefiane, V. Koutsos, and M. E. Shanahan, “Biodrop” evaporation and ring-stain deposits: The significance of dna length, *Langmuir* **32**, 4361 (2016).
- [17] F. Smith and D. Brutin, Wetting and spreading of human blood: recent advances and applications, *Curr. Opin. Colloid Interface Sci.* **36**, 78 (2018).
- [18] M. Beigtan, Y. Hwang, and B. M. Weon, Inhibiting cracks in latte droplets, *Langmuir* **39**, 5275 (2023).
- [19] S. K. Wilson and H.-M. D’Ambrosio, Evaporation of sessile droplets, *Annu. Rev. Fluid Mech.* **55**, 481 (2023).
- [20] D. Lohse and X. Zhang, Surface nanobubbles and nanodroplets, *Rev. Mod. Phys.* **87**, 981 (2015).
- [21] H. Y. Erbil, Evaporation of pure liquid sessile and spherical suspended drops: A review, *Adv. Colloid Interface Sci.* **170**, 67 (2012).
- [22] E. Sultan, A. Boudaoud, and M. B. Amar, Evaporation of a thin film: diffusion of the vapour and marangoni instabilities, *J. Fluid Mech.* **543**, 183 (2005).
- [23] G. Dunn, S. Wilson, B. Duffy, S. David, and K. Sefiane, A mathematical model for the evaporation of a thin sessile liquid droplet: Comparison between experiment and theory, *Colloids Surf., A* **323**, 50 (2008).
- [24] A. W. Wray and M. R. Moore, Evaporation of non-circular droplets, *J. Fluid Mech.* **961**, A11 (2023).
- [25] V. Dubey, Evaporation of confined droplet between parallel chips with varying gap at room temperature, *J. Micromech. Microeng.* **32**, 075001 (2022).
- [26] L. Bansal, S. Hatte, S. Basu, and S. Chakraborty, Universal evaporation dynamics of a confined sessile droplet, *Appl. Phys. Lett.* **111**, 101601 (2017).
- [27] Y. Kim, M. Gonçalves, D.-H. Kim, and B. M. Weon, Topological heterogeneity and evaporation dynamics of irregular water droplets, *Sci. Rep.* **11**, 18700 (2021).
- [28] P. Sáenz, A. Wray, Z. Che, O. Matar, P. Valluri, J. Kim, and K. Sefiane, Dynamics and universal scaling law in geometrically-controlled sessile drop evaporation, *Nat. Commun.* **8**, 14783 (2017).
- [29] M. J. Neeson, R. R. Dagastine, D. Y. Chan, and R. F. Tabor, Evaporation of a capillary bridge between a particle and a surface, *Soft Matter* **10**, 8489 (2014).
- [30] S. J. Lim, D. Kim, Y. Kim, S. Jeong, C. Pang, S. Ryu, and B. M. Weon, Hydrophobicity evolution on rough surfaces, *Langmuir* **36**, 689 (2020).
- [31] K. Cho, I. G. Hwang, Y. Kim, S. J. Lim, J. Lim, J. H. Kim, B. Gim, and B. M. Weon, Low internal pressure in femtoliter water capillary bridges reduces evaporation rates, *Sci. Rep.* **6**, 22232 (2016).
- [32] M. Gonçalves, J. Y. Kim, Y. Kim, N. Rubab, N. Jung, T. Asai, S. Hong, and B. M. Weon, Droplet evaporation on porous fabric materials, *Sci. Rep.* **12**, 1087 (2022).
- [33] Y. Dong, L. Wang, and C. Wei, Characterization of liquid-vapor interfaces in pores during evaporation, *Water Resour. Res.* **58**, e2021WR031908 (2022).
- [34] H. K. Park, Y. Kim, H. Min, C. Pang, and B. M. Weon, Hexagonal deposits of colloidal particles, *Phys. Rev. E* **100**, 022602 (2019).
- [35] E. Shahræeni and D. Or, Pore-scale evaporation-condensation dynamics resolved by synchrotron x-ray tomography, *Phys. Rev. E* **85**, 016317 (2012).
- [36] M. Scheel, R. Seemann, M. Brinkmann, M. Di Michiel, A. Sheppard, B. Breidenbach, and S. Herminghaus, Morphological clues to wet granular pile stability, *Nat. Mater.* **7**, 189 (2008).
- [37] R. N. Wenzel, Resistance of solid surfaces to wetting by water, *Ind. Eng. Chem.* **28**, 988 (1936).
- [38] A. Cassie and S. Baxter, Wettability of porous surfaces, *Trans. Faraday Soc.* **40**, 546 (1944).
- [39] Y. Nagata, K. Usui, and M. Bonn, Molecular mechanism of water evaporation, *Phys. Rev. Lett.* **115**, 236102 (2015).
- [40] See Supplemental Material at <http://link.aps.org/supplemental/10.1103/PhysRevResearch.6.L012026> for the details of the experimental assumption for the analysis, results, and the representative experimental movies about the evaporation dynamics of confined nonspherical droplets.

- [41] L. Yang, Y. Tu, and H. Fang, Modeling the rupture of a capillary liquid bridge between a sphere and plane, *Soft Matter* **6**, 6178 (2010).
- [42] N. Maeda, J. N. Israelachvili, and M. M. Kohonen, Evaporation and instabilities of microscopic capillary bridges, *Proc. Natl. Acad. Sci. USA* **100**, 803 (2003).
- [43] H. Hu and R. G. Larson, Evaporation of a sessile droplet on a substrate, *J. Phys. Chem. B* **106**, 1334 (2002).
- [44] R. D. Deegan, O. Bakajin, T. F. Dupont, G. Huber, S. R. Nagel, and T. A. Witten, Contact line deposits in an evaporating drop, *Phys. Rev. E* **62**, 756 (2000).